Journal of Materials Chemistry A

Accepted Manuscript

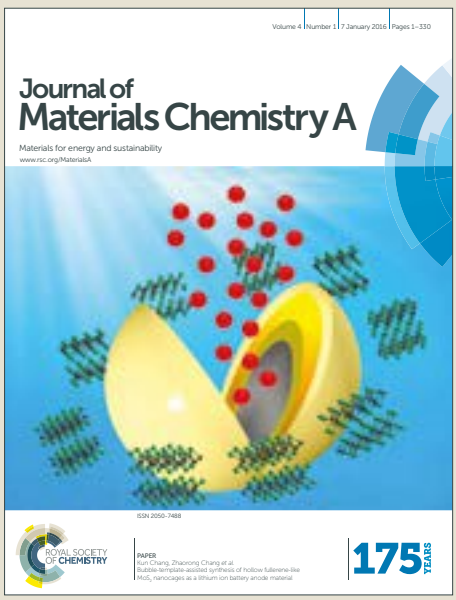

ROYAL SOCIETY OF CHEMISTRY

rsc.li/materials-a

View Article Online
DOI: 10.1039/C8TA04774J

Pyrazine Incorporated Panchromatic Sensitizers for Dye Sensitized Solar Cells under One Sun and Dim Light

Mulu Berha Desta,[a,b,c,d] *Nguyễn So'n Vinh,*[e] *CH Pavan Kumar,*[a] *Sumit Chaurasia,*[a] *Wei-Ti Wu,*[a] *Jiann T. Lin,*[a]* *Tzu-Chien Wei,*[e]* *Eric Wei-Guang Diau*[c]

[a]Institute of Chemistry, Academia Sinica, Nankang, Taipei−115, Taiwan

[b]Taiwan International Graduate Program (TIGP), Sustainable Chemical Science and Technology (SCST), Academia Sinica, Taipei, Taiwan

[c]Department of Applied Chemistry, National Chiao Tung University, Hsinchu, Taiwan

[d]Department of Chemistry, Mekelle University, Mekelle, Ethiopia

[e]Department of Chemical Engineering, National Tsing Hua University, Hsinchu 300, Taiwan

jtlin@gate.sinica.edu.tw, tcwei@mx.nthu.edu.tw

ORCID ID: 0000-0002-9704-5322 (Lin); 0000-0002-9608-8275 (Wei)

Abstract: New D−A′−π−A type (D = electron donor, A′ = auxiliary acceptor, π = π-conjugated bridge, A = electron acceptor/anchor) sensitizers with two bis(alkoxy)phenyl substituents incorporated thieno[3,4-*b*]pyrazines (**TP**) or benzo[3,4-*b*]pyrazine (**BP**) entity as the auxiliary acceptor have been synthesized for dye-sensitized solar cells (DSSCs) application. Under 1 sun illumination, the DSSCs fabricated from the two **BP** dyes with co-adsorbent have efficiencies of 8.39% and 9.03%, respectively. The latter surpasses that of the standard N719 dye (8.87%). Under dim light condition MD7 exhibited a power conversion efficiency of 18.95% and 27.17% under 300 lux and 6000 lux irradiance, respectively.

Keywords: Pyrazines; Electron deficient entities; Metal-free sensitizers; Dye-Sensitized Solar Cells, Dim-light.

View Article Online
DOI: 10.1039/C8TA04774J

1 Introduction

In recent years, the drastic improvement in efficiency[1] of metal-free dye-sensitized solar cells (DSSCs)[2] has paved a path leading to their commercialization parallel to conventional Si-based solar cells. Compared with Si-based solar cells, DSSCs have an immense potential owing to their flexibility in molecular design, easy device fabrication, environmental friendliness and low cost of production.[3] A high power conversion efficiency (PCE) of 13% has achieved with metal-free dye[1b] and Zn-porphyrin dyes.[1c] The record PCEs have also been achieved for a co-dyed single cell (14.3%)[1e] and a tandem cell (14.64%),[1j] respectively, using cobalt-based redox mediator. These values are very close to the threshold required for commercialization (15%). In order to further boost performance of DSSCs under 1 sun, sensitizers with absorption extending to near-infrared (NIR) region (~700−1400 nm) is very important as NIR light (700−2500 nm) constitutes ~50% of solar spectrum. Among NIR sensitizers, the most representative dyes are porphyrins and phthalocyanines.[4] Though the Si solar cell (absorbing in the range of 350−1000 nm) has excellent efficiency under 1 sun illumination, it is outperformed by DSSCs under dim light condition because of two reasons: (1) indoor light sources such as fluorescence lamps and white LED lights cover mainly the visible region from 400 to 650 nm; (2) being an indirect band gap material, Si solar cells need intense light illumination for efficient light harvesting. Currently DSSCs are deemed promising under indoor applications such as powering portable electronics (sensors, wireless transmitters, etc.) used in the Internet of Things (IoTs).[3a,5] However, there are only limited reports on dye-sensitized photovoltaics under indoor lighting.[6]

In this research, we intended to develop metal-free sensitizers for both indoor and outdoor DSSCs. We figured that dyes with panchromatic absorption in the visible region up to ~650 nm could cover the spectrum of T5 or white LED light source. In order to achieve this goal, we set out to develop D−A′−π−A (D = electron donor, A′ = auxiliary acceptor, π = π-conjugated bridge, A = electron acceptor/anchor) type sensitizers.[7] Incorporation of an electron deficient entity as auxiliary acceptor in the conjugated spacer of D−π−A dyes is beneficial for red shifting the absorption spectra due to deepened LUMO and improving the photostability of sensitizers. We reckon that A′ is like a double-edged blade: on one hand, it helps with red shifting the absorption spectra; on the other hand, it deteriorates electron injection of the excited dye molecule due to charge trapping.[8] Therefore, proper design of the conjugated spacers with A′ are needed for good performance of DSSCs. For example, replacing benzothiadiazole (**BT**)[9] with more electron

View Article Online
DOI: 10.1039/C8TA04774J

deficient pyrido[2,1,3]thiadiazole (**PyT**)[10] resulted in lower cell performance in spite of the longer wavelength ICT band. In comparison, the cell performance was improved by one order when **PyT** was replaced with less electron deficient 2*H*-[1,2,3]triazolo[4,5-*c*]pyridine (**PT**).[11] Similarly, replacing pyridoimidazole (**PIm**) by 1*H*-benzo[*d*]imidazole (**BIm**) led to better cell efficiency.[12] We therefore set out to develop D−A′−π−A type sensitizers with benzo[3,4-*b*]pyrazine (**BP**), an electron-withdrawing entity popularly used for small band gap D−A type polymeric materials,[13] as the auxiliary acceptor (A′). The **BP** was selected as its moderate electron deficiency[7b] may avoid spectral over red shift of the dye and charge trapping of the excited dye molecule. More electron deficient entity, thieno[3,4-*b*]pyrazines (**TP**), was also chosen as the electron-withdrawing entity for comparison. Incorporation of alkyl or aryl substituents at the pyrazine ring of **BP** or **TP** allows tuning the solubility and optical property of the dyes.[14] Herein we incorporate 3,4-dihexyloxyphenyl moiety at the 2- and 3-site of **BP** and **TP** to alleviate serious dye aggregation. To our knowledge, D−A′−π−A dyes incorporating dialkoxyphenyl unit at the auxiliary acceptor have not been reported so far, though there were examples of dyes with 2,4-dialkoxyphenyl moiety at the donor.[15] In addition to ambient light, the DSSCs fabricated from the new dyes were also explored under 1 sun. The result shows these novel dyes perform well in both 1 sun irradiation and 300 lux T5 fluorescent light, providing viable materials for realizing practical use of DSSC.

2 Experimental Section

2.1 Materials and Characterizations

All commercially purchased solvents were dried before use. Reactions were performed under inert atmosphere using standard Schlenk techniques unless specified. ^{1}H and ^{13}C NMR spectra were recorded on a Bruker AVA-300 and AVIII-400 spectrometer. UV-vis absorption spectra of dyes in solution and on mesoporous TiO_2 films were measured using Cary 300 Bio UV-vis spectrophotometer (Varian) and photoluminescence measurements were carried out with a HITACHI F-4500 fluorescence spectrophotometer. Cyclic voltammetry (CV) measurements were performed on a CHI-621A potentiostat (CH-Instruments, Inc.), Pt-wire as the counter electrode and Ag/AgCl electrode as the reference electrode at a scan rate of 50 mV s^{-1}. Tetra *n*-butylammonium hexafluorophosphate and THF were used as the supporting electrolyte and solvent, respectively. Elemental analysis was performed on a PerkinElmer 2400 analyzer. Fast atom bombardment mass spectrometry (FAB MS) analysis was performed on a JEOL Tokyo Japan

View Article Online
DOI: 10.1039/C8TA04774J

JMS-700 mass spectrometer equipped with the standard FAB source. Photovoltaic parameters of the DSSCs were measured by a potentiostat/galvanostat (CHI650B, CH Instruments, Inc.) at 100 mW cm^{-2} (1 sun) light illumination by using a class A quality solar simulator (XES–301S, AM1.5G, San–Ei Electric Co., Ltd., Osaka, Japan). The incident light intensity of 100 mW cm^{-2} was calibrated with a standard Si cell (PECSI01, Peccell Technologies, Inc., Kanagawa, Japan). Incident photon–to–current conversion efficiencies (IPCE) of the DSSCs were recorded by the same potentiostat/galvanostat under monochromatic light illumination in a wavelength range of 380-900 nm. To obtain the IPCE data, another class-A solar simulator (PEC–L11, AM1.5G, Peccell Technologies, Inc., Kanagawa, Japan) equipped with a monochromator (model 74100, Oriel Instrument, California, USA) was used. The incident radiation flux (φ) was obtained by using an optical detector (model 818-SL, Newport, California, USA) and a power meter (model 1916-R, Newport, California, USA). Electrochemical impedance spectra (EIS) of DSSCs were recorded by the same potentiostat/galvanostat equipped with a FRA2 module at an applied voltage of -0.70 V. The explored frequency range is set from 10 MHz to 100 kHz with an AC amplitude of ±10 mV using an equipped FRA2 module. The TiO_2 nanoparticles and the reference dye of N719 were purchased from Solaronix, S.A., Switzerland.

2.2 Experimental Procedures

The synthesis of 1,2-bis(3,4-bis(hexyloxy)phenyl)ethane-1,2-dione, 3,6-dibromobenzene-1,2-diamine, [2,2':5',2''-terthiophene]-3',4'-diamine are described in supporting information. The syntheses of dyes and relevant precursors are also described in Supporting Information except for **MD4**.

*Synthesis of 2,3-bis(3,4-bis(hexyloxy)phenyl)-5,7-di(thiophen-2-yl)thieno[3,4-b]pyrazine (**4a**)*: A mixture of 1,2-bis(3,4-bis(hexyloxy)phenyl)ethane-1,2-dione (3.0 mmol, 1.83 g), [2,2':5',2''-terthiophene]-3',4'-diamine (3.0 mmol, 0.83 g), and *para*-toluenesulfonic acid (0.2 mmol) in dry $CHCl_3$ was refluxed for 12 h and monitored through TLC. On completion, the reaction mixture was cooled to room temperature and then poured into the crushed ice, and finally extracted with DCM (100 mL x 3). The organic extracts were combined and dried over anhydrous $MgSO_4$. The crude product was purified by flash column chromatography using hexane: DCM (1:4 by vol.) as the eluent. Compound **4a** was obtained as a red solid (82% yield). ^{1}H NMR (400 MHz, $CDCl_3$): δ 0.91-0.98 (m, 12H), 1.33-1.41 (m, 16H), 1.43-1.53 (m, 8H), 1.74-1.89 (m, 8H), 3.91 (t, J = 6.5 Hz,

View Article Online
DOI: 10.1039/C8TA04774J

4H), 4.04 (d, *J* = 6.5 Hz, 4H), 6.85 (d, *J* = 8.4 Hz 1H), 7.12-7.16 (m, 2H), 7.20 (d, *J* = 8.4 Hz, 2H), 7.25-7.27 (m, 2H), 7.39 (d, *J* = 5.0 Hz, 2H), 7.66-7.68 (m, 2H). MS (HRMS): m/z calculated for $C_{50}H_{64}N_2O_4S_3$ [M] 852.4028; found $[M + H]^+$ 853.4110.

*Synthesis of 5-(2,3-bis(3,4-bis(hexyloxy)phenyl)-7-(thiophen-2-yl)thieno[3,4-b]pyrazin-5-yl)thiophene-2-carbaldehyde (**4b**):* 2,3-Bis(3,4-bis(hexyloxy)phenyl)-5,7-di(thiophen-2-yl)thieno[3,4-*b*]pyrazine (2.35 mmol, 2.0 g) was dissolved in dry DMF (10 ml) and the solution was cooled to 0 ^oC. Phosphorous oxychloride (2.81 mmol, 0.263 ml) was added to the solution dropwise at 0 ^oC and then the solution was warmed slowly to room temperature and then stirred at 80 ^oC for overnight. After completion, the reaction mixture was poured into ice water (200 mL) and stirred for 10 minutes, extracted with DCM (100 mL x 3). The organic layer was combined and dried over anhydrous $MgSO_4$. After filtration, the solvent of the filtrate was removed under reduced pressure, and the product was purified by flash column chromatography using hexane: DCM (1:4 by vol.) as the eluent. Compound **4b** was obtained as a dark red solid (72% yield). ^1H NMR (400 MHz, $CDCl_3$): δ 0.91-0.98 (m, 12H), 1.33-1.42 (m, 16H), 1.44-1.56 (m, 8H), 1.76-1.91 (m, 8H), 3.89-3.95 (m, 4H), 4.02-4.09 (m, 4H), 6.87 (t, *J* = 8.3 Hz, 2H), 7.15 (t, *J* = 4.00 Hz, 1H), 7.22 (d, *J* = 8.3 Hz, 1H), 7.25-7.29 (m, 3H), 7.45 (d, *J* = 5.00 Hz, 1H), 7.63 (d, *J* = 4.00 Hz, 1H), 7.71 (m, 2H), 9.93 (s, 1H). MS (FAB) m/z: 881.6 (M^+).

*Synthesis of 5-(2,3-bis(3,4-bis(hexyloxy)phenyl)-7-(5-bromothiophen-2-yl)thieno[3,4-b]pyrazin-5-yl)thiophene-2-carbaldehyde (**4c**)*: 5-(2,3-Bis(3,4-bis(hexyloxy)phenyl)-7-(thiophen-2-yl)thieno[3,4-*b*]pyrazin-5-yl)thiophene-2-carbaldehyde **4b** (1.59 mmol, 1.4 g) was dissolved in dry DMF (20 mL) and the mixture was cooled to 0 ^oC. NBS (1.75 mmol, 283 mg) was added slowly to the solution and the reaction mixture was warmed slowly and stirred for 12 h. Finally, the reaction mixture was poured into ice water and extracted with DCM (100 mL x 2). The organic extracts were combined and dried over anhydrous $MgSO_4$. After filtration, the solvent of the filtrate was removed under reduced pressure and the residue was purified by flash column chromatography using hexane: CH_2Cl_2 (1:4 by vol.) as the eluent. Compound **4c** was obtained as a brown solid (68% yield). ^1H NMR (300 MHz, $CDCl_3$): δ 0.84-0.95 (m, 12H), 1.32-1.60 (m, 24H), 1.81-1.95 (m, 8H), 3.95-4.06 (m, 8H), 6.77-6.84 (m, 2H), 7.02 (s, 1H), 7.11-7.21 (m, 2H), 7.38-7.42 (m, 2H), 7.64 (s, 1H), 9.84 (s, 1H). MS (MALDI) m/z: 961.3 $[M+ H]^+$.

View Article Online
DOI: 10.1039/C8TA04774J

*Synthesis of 5-(2,3-bis(3,4-bis(hexyloxy)phenyl)-7-(5-(4-(diphenylamino)phenyl)thiophen-2-yl)thieno[3,4-b]pyrazin-5-yl)thiophene-2-carbaldehyde (**4d**)*: To a flame dried flask 5-(2,3-bis(3,4-bis(hexyloxy)phenyl)-7-(5-bromothiophen-2-yl)thieno[3,4-*b*]pyrazin-5-yl)thiophene-2-carbaldehyde **4c** (0.94 mmol, 0.90 g), *N*,*N*-diphenyl-4-(tributylstannyl)aniline (1.41 mmol, 0.75 g) and $PdCl_2(PPh_3)_2$ (0.02 mmol, 13 mg) was added 20 mL of dry DMF via syringe and the mixture was stirred under nitrogen atmosphere at 100 ^oC for 15 h. Reaction was also monitored through TLC. After completion of the reaction, the mixture was poured into ice water (200 mL) and extracted with CH_2Cl_2 (100 mL x 3). The organic extracts were combined, washed with brine, and dried over anhydrous $MgSO_4$. Product **4d** was obtained in 58% yield by flash column chromatography using hexane: CH_2Cl_2 (1:4 by vol.) as the eluent. ^1H NMR (400 MHz, $CDCl_3$): δ 0.83-0.93 (m, 12H), 1.21-1.28 (m, 4H), 1.29-1.39 (m, 14H), 1.40-1.51 (m, 6H), 1.68-1.88 (m, 8H), 6.79 (d, J = 8.5 Hz, 1H), 6.85 (d, J = 8.5 Hz, 1H), 7.03-7.07 (m, 4H), 7.11-7.15 (m, 5H), 7.21-7.32 (m, 8H), 7.50 (d, J = 8.5 Hz, 2H), 7.60 (d, J = 4.0 Hz, 1H), 7.65 (d, J = 4.0 Hz, 1H), 7.69 (d, J = 4.0 Hz, 1H), 9.88 (m, 1H). MS (MALDI) m/z: 1124.5 $[M + H]^+$.

Synthesis of 5-(7-(5-(4-(bis(4-(hexyloxy)phenyl)amino)phenyl)thiophen-2-yl)-2,3-bis(3,4-bis(hexyloxy)phenyl)thieno[3,4-b]pyrazin-5-yl)thiophene-2-carbaldehyde (**4e**):

The synthetic procedure was similar to that of **4d** except that 4-(hexyloxy)-*N*-(4-(hexyloxy)phenyl)-*N*-(4-(tributylstannyl)phenyl)aniline was used instead of *N*,*N*-diphenyl-4-(tributylstannyl)aniline. The crude product was purified by flash chromatography using hexane: CH_2Cl_2 (1:2 by vol.) as the eluent to afford **4e** as a brown solid (80% yield). ^1H NMR (400 MHz, $CDCl_3$): δ 0.94-0.97 (m, 18H), 1.36-1.40 (m, 24H), 1.49-1.52 (m, 12H), 1.78-1.87 (m, 12H), 3.93-3.98 (m, 8H), 4.04-4.08 (m, 4H), 6.80-6.93 (m, 14H),7.09-7.14 (m, 2H), 7.23 (s, 1H), 7.25-7.45 (m, 3H), 7.51 (s, 1H), 7.60-7.61 (m, 1H), 9.85 (s, 1H). MS (FAB): m/z calculated for $C_{81}H_{101}N_3O_7S_3$ [M] 1323.68; found $[M + H]^+$ 1324.70.

*Synthesis of 3-(5-(2,3-bis(3,4-bis(hexyloxy)phenyl)-7-(5-(4-(diphenylamino)phenyl)thiophen-2-yl)thieno[3,4-b]pyrazin-5-yl)thiophen-2-yl)-2-cyanoacrylic acid (**MD4**)*: 5-(2,3-bis(3,4-bis(hexyloxy)phenyl)-7-(5-(4-(diphenylamino)phenyl)thiophen-2-yl)thieno[3,4-*b*]pyrazin-5-yl)thiophene-2-carbaldehyde **4d** (0.27 mmol, 0.30 g), 2-cyanoacetic acid (0.40 mmol, 34 mg), ammonium acetate (10 mg) and acetic acid (10 mL) were mixed in two neck round bottom flask under nitrogen and stirred at 100 ^oC for 12 h. The solution was cooled to room temperature and poured into ice water (100 mL) and extracted with CH_2Cl_2 (100 mL x 2). The organic layer was

View Article Online
DOI: 10.1039/C8TA04774J

combined and dried over anhydrous $MgSO_4$. After filtration, the solvent of the filtrate was removed under reduced pressure and crude product was purified by flash column chromatography using 1% acetic acid in CH_2Cl_2 as the eluent. Compound **MD4** was obtained as a dark green solid (56% yield). ^{1}H NMR (400 MHz, THF-d_8): δ 0.86-0.98 (m, 12H), 1.25-1.70 (m, 28H), 1.71-1.92 (m, 4H), 3.74 (t, J = 6.4 Hz, 2H), 3.88 (t, J = 6.0 Hz, 2H), 4.02 (t, J = 6.6 Hz, 2H), 4.13 (t, J = 6.4 Hz, 2H), 6.78 (d, J = 8.3 Hz, 1H), 6.95-6.97 (m, 4H), 7.05-7.11 (m, 8H), 7.25-7.36 (m. 10H), 7.55 (m, 1H), 7.72 (d, J = 7.2 Hz, 1H), 8.26 (s, 1H). ^{13}C NMR (75 MHz, THF-d_8): δ 14.09, 22.67, 25.76, 29.30, 31.61, 69.04, 69.40, 122.75, 123.43, 124.85, 126.27, 127.59, 129.40, 147.24, 147.49, 148.82, 149.55, 162.39. MS (FAB): m/z calcd. for $C_{72}H_{78}N_4O_6S_3$ [M]: 1190.5083 found: $[M+H]^+$ 1191.5173.

2.3 Fabrication of DSSC

Dye-sensitized solar cells were fabricated using conductive glass, fluorine-doped tin oxide (FTO, TEC-7, 7 Ω/sq, NSG America Inc., New Jersey, USA), as the substrate for photoanode and counter-electrode (CE) after proper cleaning. The FTO glasses were firstly cleaned via the ultra-sonication in the bathes of neutral cleaner, de-ionized water, acetone, and isopropanol, sequentially. A 12 μm-thick TiO_2 film, containing a 7 μm-thick transparent layer (Solarnix transparent paste) and a 5 μm-thick scattering layer, was casted on the cleaned FTO with a controlled area of 0.16 cm^2 and was sintered at 450 ^{o}C for 30 min in an air atmosphere.[16] The film thickness is measured by a profilometer (Dektak3, Veeco/Sloan Instruments Inc., USA). The sintered TiO_2 film was immersed in 3×10^{-4} M dye solution at room temperature for 12 h in THF. For the cases of the dyes co-adsorbed with chenodeoxycholic acid (CDCA), 1 mM of CDCA is added into each dye solution. After rinsing with acetonitrile, the dye-adsorbed TiO_2 photoanode was obtained. Finally, a photoanode was assembled with a sputtered-platinum/FTO counter electrode using a 25 μm-thick Surlyn® (SX1170-25, Solaronix S. A., Switzerland) as the cell spacer. The iodide-based electrolyte, containing 0.1 M lithium iodide (LiI), 1.0 M 1,2-dimethyl-3-propylimidazolium iodide (DMPII), 0.04 M iodine (I_2), and 0.5 M 4-*tert*-butylpyridine (TBP) in acetonitrile/3-methoxypropionitrile (ACN/MPN = 8:2 by vol.), was injected into the cell gap between these two electrodes by capillarity. The cell parameters for the dim light irradiation have been adjusted as follows: a mesoporous TiO_2 (12 μm active layer ~ 4 μm-thick scattering layer)

View Article Online
DOI: 10.1039/C8TA04774J

with an effective area of 0.16 cm^2 and a redox electrolyte composition of LiI (0.3 M), I_2 (0.5 M), DPMII (1M) and TBP (0.5 M) in ACN/MPN (80:20 v/v).

2.4 Computational Details

All the calculations have been performed using the Gaussian 09 program package.[17] Geometrical optimization was performed in vacuo using B3LYP exchange-correlation functional and a 6-311G (d,p)[18] basis set. The optimized geometries were then used to obtain frontier molecular orbitals (FMOs). To simulate the optical spectra, the lowest spin allowed singlet-singlet transitions were computed on the ground state geometry. TDDFT calculations of the lowest singlet-singlet excitations were performed in THF solution, on the optimized geometries using the CAM-B3LYP/6-311G (d,p) level of theory. The integral equation formalism polarizable continuum model (PCM)[19] within self-consistent reaction field (SCRF) theory, has been used to describe the solvation of the dyes. The TDDFT calculations were also performed using CAM-B3LYP with a 6-311G (d, p) basis set. The software GaussSum 2.2.5 was utilized to simulate the major portion of absorption spectrum and to analyze the nature of transitions.[20]

3 Results and Discussion

3.1 Synthesis and Characterization

The structures of the new sensitizers are shown in **Fig. 1**, and **Schemes 1** and **2** describe the synthetic pathway for **MD4**/**MD6** and **MD5**/**MD7** respectively. Pyrazine cores (**4a**, **5a**) were synthesized by refluxing a mixture of the corresponding diamine[21] and diketone[22] in suitable solvent as mentioned in the schemes. It is worth noting that we failed to isolate dihexyloxyphenyl moiety-free analogues of **4**a and **5a**, possibly due to low solubility of intermediates stemmed from serious intermolecular aggregation. Vilsmeier-Haack reaction was performed on **4a** to provide aldehyde intermediate, **4b**, which underwent subsequent bromination with NBS to afford **4c**. Next, Stille cross coupling reaction between **4c** and *N*,*N*-diphenyl-4-(tributylstannyl)aniline[23] was carried out to incorporate the arylamine donor, and subsequent Knoevenagel condensation reaction furnished the desired **MD4** dye. Stille cross coupling of tributyl(thiophen-2-yl)stannane[23] with **5a** afforded **5b**, which then underwent formylation to give **5c** via Vilsmeier-Haack reaction. Subsequent bromination of **5c** with NBS provided **5d**. Stille cross coupling reaction of **5d** with *N*,*N*-diphenyl-4-(tributylstannyl)aniline afforded **5e** incorporating the donor group, which

View Article Online
DOI: 10.1039/C8TA04774J

underwent subsequent Knoevenagel condensation with cyanoacetic acid to provide **MD5**. The synthetic procedure of **MD6** and **MD7** was similar to that of **MD4** and **MD5** except that 4-(hexyloxy)-*N*-(4-(hexyloxy)phenyl)-*N*-(4-(tributylstannyl)phenyl)aniline was used instead of *N*,*N*-diphenyl-4-(tributylstannyl)aniline.

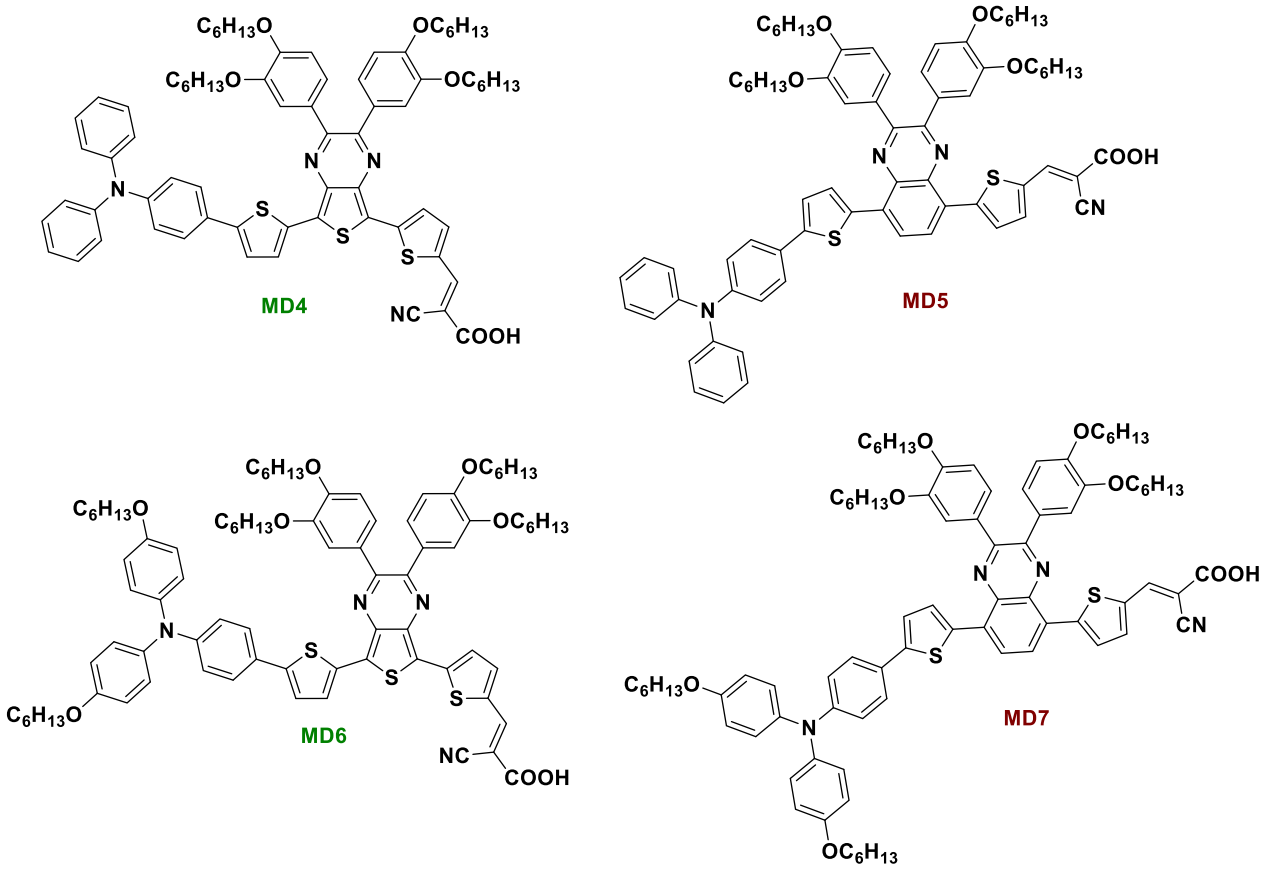

Fig. 1 Molecular structures of the pyrazine-based **MD4**–**MD7** dyes

View Article Online
DOI: 10.1039/C8TA04774J

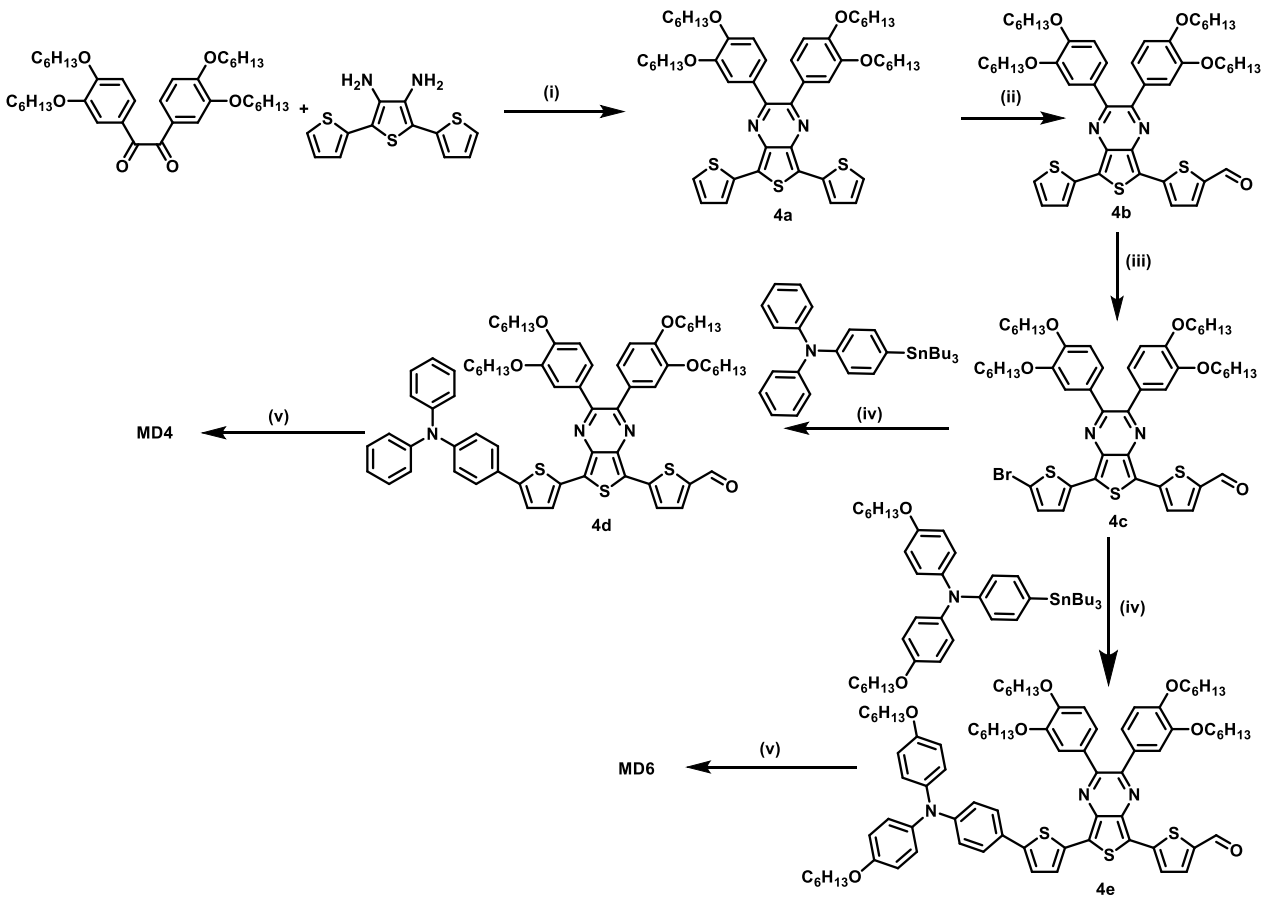

Scheme 1 Synthetic route of MD4 and MD6 dyes. (i) PTSA, $CHCl_3$, reflux, 12 h; **(ii)** $POCl_3$, DMF, 0-80 ^oC, 12 h; **(iii)** NBS, DMF, 0 ^oC, 12 h; **(iv)** $PdCl_2(PPh_3)_2$, 80 ^oC, DMF, 15 h; **(v)** $CNCH_2COOH$, NH_4OAc, AcOH, 100 ^oC, 15 h.

View Article Online
DOI: 10.1039/C8TA04774J

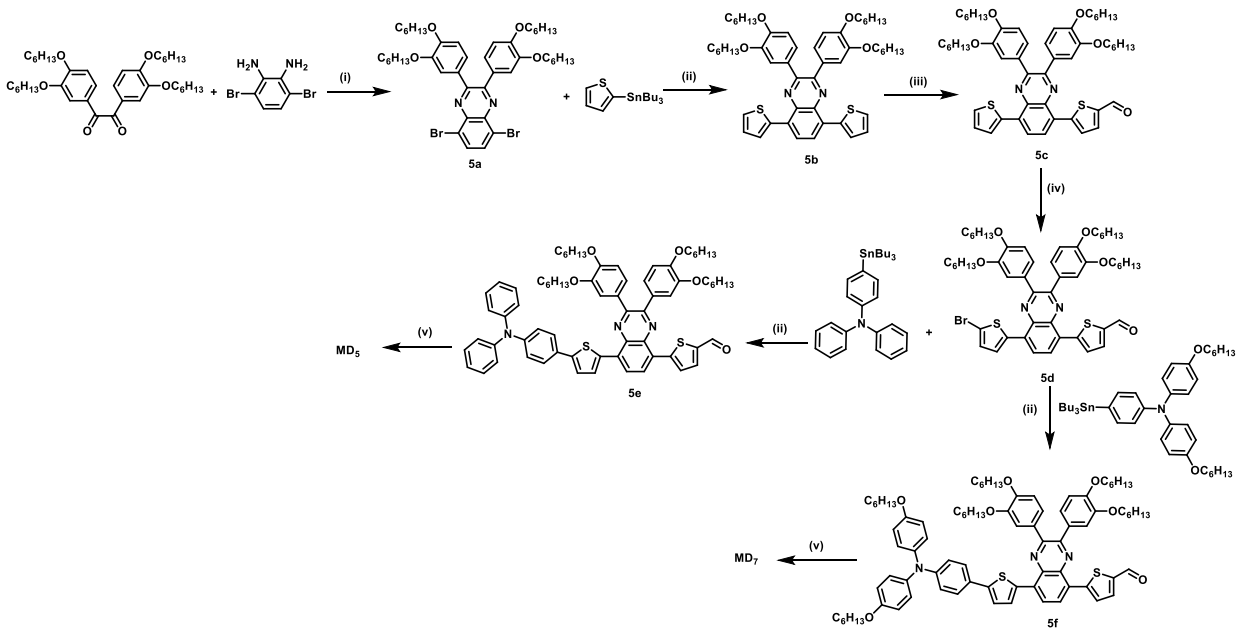

Scheme 2: Synthetic route of MD5 and MD7 dyes. (i) Ethanol, AcOH, refilux, 12 h; **(ii)** $PdCl_2(PPh_3)_2$, 100 ^oC, DMF,15 h; **(iii)** $POCl_3$, DMF, 0-80 ^oC, 12 h; **(iv)** NBS, DMF, 0 ^oC, 12 h; **(v)** $CNCH_2COOH$, NH_4OAc, AcOH, 100 ^oC, 15 h.

3.2 Photophysical and Electrochemical Characteristics

The UV−vis absorption spectra of **MD** dyes were measured in THF and on TiO_2 film (**Fig. 2a** and **2b**) and the optical HOMO/LUMO energy gap of the dyes were estimated from the intersection of normalized absorption and fluorescence spectra. The dyes show panchromatic absorption: an intense band at the higher energy region is attributed to π–π* transition and a broad intramolecular charge transfer (ICT) band appears at the longer wavelength region. The thieno[3,4-*b*]pyrazine-based dyes, **MD4** and **MD6**, show absorption maxima (λ_{max}) at 633 nm and 642 nm with the λ_{onset} reaching >750 nm (**Fig. 2**, **Table 1**) and the molar absorption coefficient exceeding 10000 $M^{-1}cm^{-1}$ at 700 nm. Compared with **MD4** and **MD6**, the absorption maxima of **MD5** (513 nm) and **MD7** (532 nm) are blue-shifted by 120 nm and 110 nm respectively, which is consistent with the more electron deficient nature of thieno[3,4-*b*]pyrazine (in **MD4** and **MD6**) than benzo[3,4-*b*]pyrazine (in **MD5** and **MD7**).[24] Incorporation of the alkoxy substituents at the arylamine donor increases its strength and results in red shift of the absorption: **MD6** > **MD4** and **MD7** > **MD5**. It is noteworthy that the molar extinction coefficient of **MD4** (ε = 32,231 $M^{-1}cm^{-1}$), **MD6** (ε = 33,530 $M^{-1}cm^{-1}$), **MD5** (ε = 32,231 $M^{-1}cm^{-1}$) and **MD7** (ε = 39,360 $M^{-1}cm^{-1}$) are greater than **BP** and **TP** congeners with similar skeletons, **CR**[25] and **DJ**[26] (**BT** dyes), and **NL**[14d] and **FNE** (**TP** dyes).[27] This

View Article Online
DOI: 10.1039/C8TA04774J

can be attributed to better planarity of the conjugated skeleton and incorporation of the alkoxy substituents for the **MD** dyes. Though there is negligible dye aggregation in the solution up to concentration of 3 x 10^{-4} M in view of linearity of the absorbance vs. concentration (in THF) plot (**Fig. 2**b), slight dye aggregation still exists in the film state. **Fig. 2c** displays the absorption spectra for the dyes adsorbed on the TiO_2 film (~4 μm in thickness). Broadened absorption spectra in the longer wavelength region with bathochromic shift of λ_{onset} indicates the presence of *J*-aggregation of the dyes in the film state.[28] **MD4** (or **MD6**) appears to have higher tendency to aggregate than its **BP** congener (Supporting Information: **Fig. S1**), possibly due to more planar skeleton in the former. The blue shift of λ_{max} of the dyes on TiO_2 is attributed to the deprotonation of the carboxylic acid.[29]

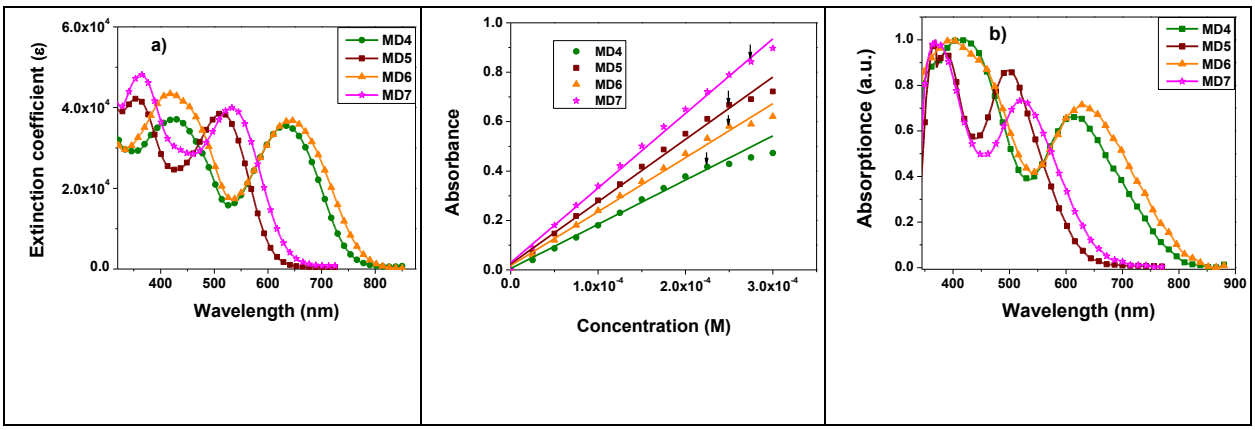

Fig. 2 (a) Absorption spectra in THF solution (10 μM), (b) absorbance vs. concentration plot in THF and (c) absorption spectra on TiO_2 thin film for **MD4**–**MD7** dyes.

To gain a better understanding of the structure-property relationship, we have carried out TDDFT studies on these dyes using CAM-B3LYP level of theory, with inclusion of the solvent (THF). A detailed list of the calculated transition energies for all the compounds are provided in the Supporting Information (**Tables S1**−**S4**), and the simulated spectra are shown in **Fig. S2**. The TDDFT results are in good agreement with the experimental UV-Vis spectra. The spectra have been produced by convoluting Gaussian functions with FWHM = 0.35 eV centered at the excitation wavenumbers. Relevant ground-state dihedral angles between aromatic entities of the conjugated skeleton are shown in **Fig. S3** (SI). There is significant twist (dihedral angles: 46.9°–43.2°) between the **BP** (or **TP**) core with its two alkoxyphenyl substituents. As expected, **TP** core

View Article Online
DOI: 10.1039/C8TA04774J

has better planarity with the neighboring thiophene rings compared with the **BP** core, and the dihedral angles are smaller in **MD4** and **MD6** (6.6°–7.7°) than in **MD5** and **MD7** (24.2°–28.3°). Selected frontier orbitals are shown in **Fig. 3** and **Fig. S4** (SI). The HOMO orbital is mainly distributed from the arylamine donor extending to the conjugated spacer, and the LUMO orbital is distributed from the anchor extending to the spacer. Charge transfer character is evident for the lowest-energy transition ($S_0 \rightarrow S_1$): >75% of HOMO → LUMO for **MD4** and **MD6**, and >50% of HOMO → LUMO for **MD5** and **MD7**. Computation on compounds **MD4'**−**MD7'**, the congeners of **MD4**−**MD7** without alkoxy chains at the **BP** or **TP** core, were also carried out in order to evaluate the influence of the alkoxy chains on the electronic property of the dyes, and the results are compiled in **Table S5**. Compared with **MD4'**−**MD7'**, **MD4**−**MD7** appear to have LUMO lowered by 0.13−0.18 eV, and therefore HOMO/LUMO gap lowered by 0.17−0.24 eV. The Mulliken charges difference between the excited-state and ground states for different segments of the **MD** dyes were also calculated from the CAM-B3LYP/6-311G for the S_1 and S_2 states in order to estimate the extent of charge separation upon excitation (**Fig. S5**). The dye molecules were grouped into several segments: the arylamine donor (D), the thiophene unit between D and **BD** or **TP** (Th-L), **BD** or **TP** (A′), the thiophene unit between A′ and the anchor (Th-R), and the anchor (A). The Mulliken charges are compiled in **Table S6**. The Mulliken charges changes at A′/A for $S_0 \rightarrow S_1$ are: **MD4**, -0.11/-0.06 |e|; **MD5**, -0.11/-0.11 |e|; **MD6**, -0.11/-0.06 |e|; and **MD7**, -0.04/-0.12 |e| respectively. The products of the oscillator strength and the Mulliken charge changes in A are as below: **MD4**, 0.06 |e|; **MD5**, 0.15 |e|; **MD6**, 0.07 |e|; and **MD7**, 0.17 |e| respectively. Therefore, the **TP**-based dyes (**MD4** and **MD6**) have more charges trapped at A′ and less charges residing at A compared with the **BP**-based dyes (**MD5** and **MD7**). This implies that electronic injection from the excited dye molecule to TiO_2 is more facile for the **BP**-based dyes.

View Article Online
DOI: 10.1039/C8TA04774J

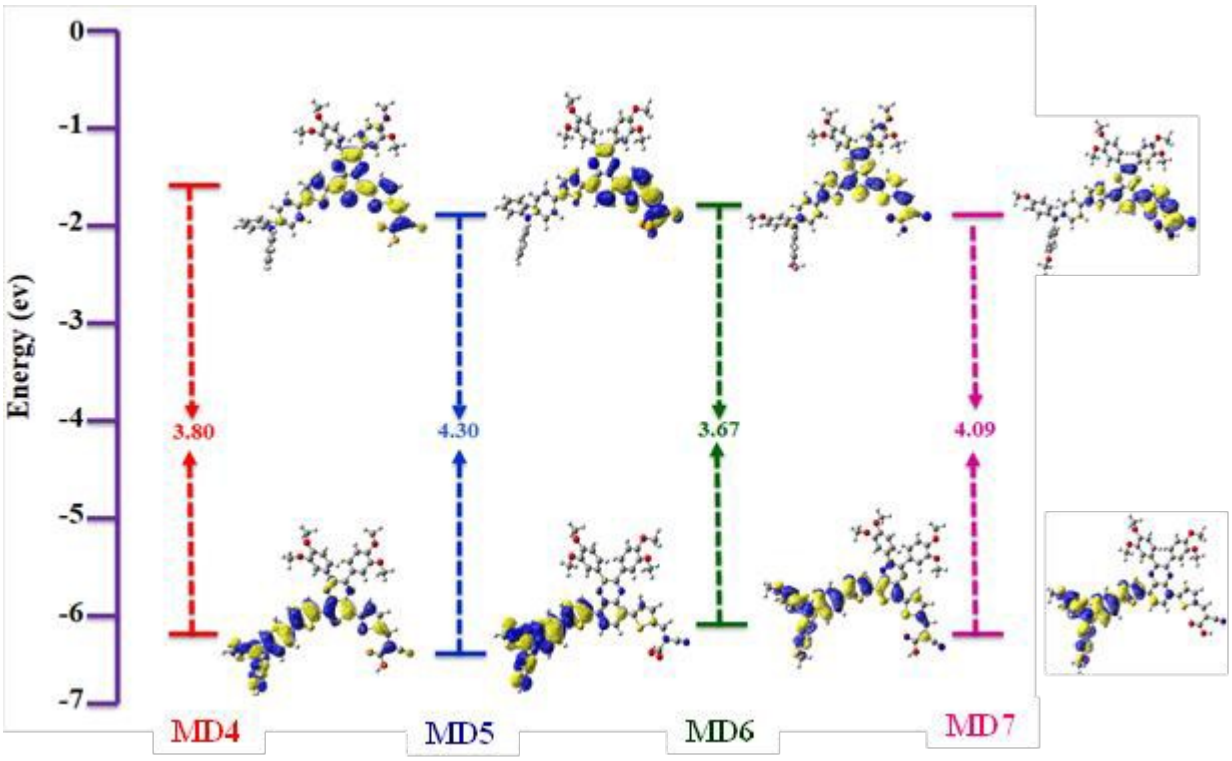

Fig. 3 HOMO and LUMO orbitals and the corresponding energies.

Table 1 Electro-optical parameters of **MD4**–**MD7** dyes

dye	λ_{abs} (ε)[a] nm (M^{-1} cm^{-1})	λ_{abs}[b] nm	λ_{onset}[b] nm	E_{ox} (ΔEp)[c] mV	E_{ox}[d] V	E_{ox}*[e] V	$E_{0\text{-}0}$ (λ)[f] eV (nm)
MD4	427 (33832), 633 (32231)	613	800	261 (122), 511 (109)	0.96	-0.80	1.76 (705)
MD5	356 (41667), 513 (37998)	498	630	360 (95)	1.06	-1.04	2.10 (590)
MD6	420(40188)	629	815	142 (86)	0.84	-0.90	1.74 (713)

View Article Online
DOI: 10.1039/C8TA04774J

	642(33530)			427 (104)			
MD7	365(47545) 532(39360)	524	660	177 (90)	0.88	-1.13	2.01 (615)

[a] Recorded in THF (solution). [b] Absorption maxima and onset wavelength on TiO_2 film. [c] Recorded in THF. scan rate = 100 mVs^{-1}; electrolyte = $[(n\text{-}C_4H_9)_4][NPF_6]$; $E_{ox} = 1/2(E_{pa} + E_{pc})$, $\Delta E_p = (E_{pa} - E_{pc})$ where E_{pa} and E_{pc} are peak anodic and cathodic potentials, respectively. Oxidation potential reported is adjusted to that of ferrocene (Fc) used as an internal reference. [d] Calculated by using the formula E_{ox} (vs. NHE) = 0.77 + E_{ox} (vs. Fc). [e] $E_{ox}^* = E_{ox} - E_{0\text{–}0}$. [f] The optical HOMO/LUMO energy gap, $E_{0\text{-}0}$, was derived from the intersection of absorption and fluorescence spectra using the formula $1240/\lambda$.

3.3 Electrochemical Properties

Cyclic voltammetry (CV) measurements generally provide information on the feasibility of the electron injection and dye regeneration. The CV measurements of **MD** dyes were carried out in THF using tetra-*n*-butylammonium hexafluorophosphate ($TBAPF_6$) as the supporting electrolyte. The cyclic voltammograms and energy levels of the sensitizers are shown in **Fig. 4a** and **4b**, respectively, and the relevant data are compiled in **Table 1**. We can observe two features: (1) incorporation of hexyloxy chains at the arylamine significantly increases the electron density and lower the oxidation potential of arylamine, i.e., **MD4** vs. **MD6** and **MD5** vs. **MD7**; (2) both **MD4** and **MD6** have two quasi-reversible oxidation waves and **MD5** and **MD7** have only one. Apparently the three electron excessive thiophene rings in **MD4** and **MD6** render the molecule more electron rich, and have higher capability to accommodate two positive charges. The HOMO levels of **MD4** (0.96 V), **MD5** (1.06 V), **MD6** (0.84 V) and **MD7** (0.88 V vs. NHE), calculated from the first oxidation potential, are more positive than the I^-/I_3^- redox couple (~0.4 V vs. NHE)[30] and ascertain the efficient dye regeneration. The LUMO energy levels of the dyes **MD4** (-0.80 V), **MD5** (-1.04 V), **MD6** (-0.90 V) and **MD7** (-1.13 V vs. NHE), calculated from $E_{ox} - E_{0\text{-}0}$, are remarkably more negative than the TiO_2 conduction band-edge energy (~-0.5 V vs. NHE),[31] ensuring favorable electron injection (see **Table 1** and **Fig. 4b**).

View Article Online
DOI: 10.1039/C8TA04774J

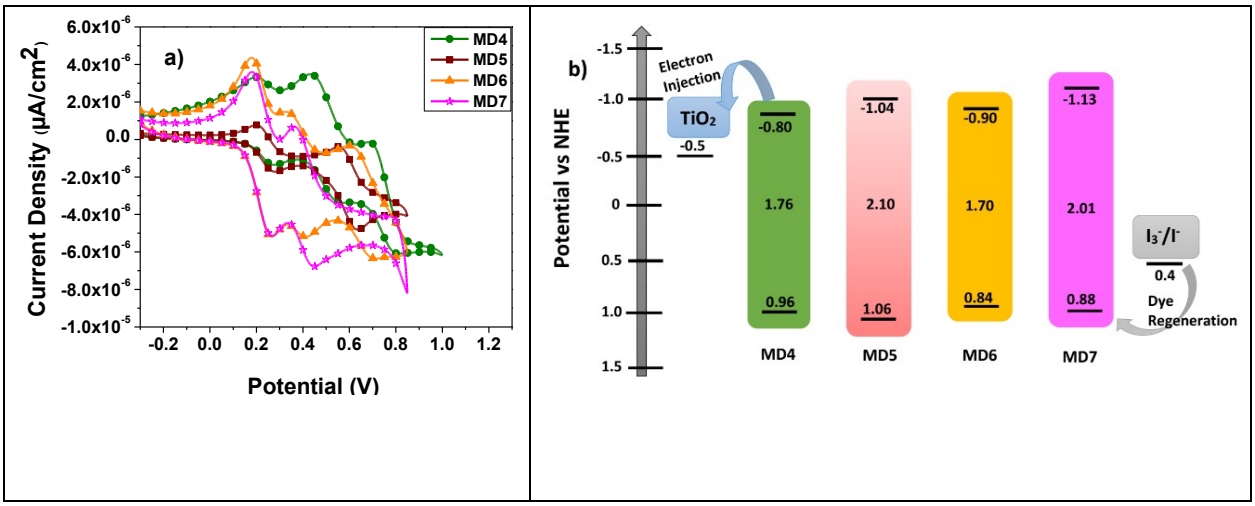

Fig. 4 (a) Cyclic Voltammograms and (b) energy-level diagram of **MD4**–**MD7** dyes.

3.4 Photovoltaic Properties

DSSCs fabricated with **MD** dyes and I^-/I_3^- redox mediator were measured under AM 1.5 G illumination. The current density−voltage (*J*−*V*) curves and the incident photon-to-current conversion efficiency (IPCE) plots of DSSCs are shown in **Fig. 5a** and **5b**, respectively. The relevant photovoltaic parameters of the cells are summarized in **Table** 2 The photocurrent densities estimated by integrating the product of the IPCE value at each wavelength and the photon flux density data listed in the AM 1.5 solar spectrum are also listed in the parentheses of the J_{SC} value for reference. They deviate from the experimental values by <15%. The dyes with **BP** core (**MD5**: 7.88%; **MD7**: 8.22%) have significantly higher performance than those with **TP** core (**MD4**: 3.92%; **MD6**: 5.08%). Compared with the solution spectra, the IPCE spectra are broadened in the longer wavelength region, which is consistent with the film spectra of the λ_{onset} (vide supra). The best performed dye, **MD7**, has IPCE values above 80% in the range of 400–620 nm. Though **MD4** and **MD6** have absorption extending to longer wavelength spectral region, their IPCE values are lower than 60%. They may stem from several reasons: (1) higher electron density is trapped at the more electron deficient **TP** entity of **MD4** and **MD6**, leading to lower electron injection efficiency (see Mulliken charge analysis, vide supra); (2) there is lower dye loading for **MD4** and **MD6**; (3) higher degree of dye aggregation in **MD4** and **MD6** due to more planar skeleton (vide supra) jeopardizes the electron injection. Moreover, **MD4** and **MD6** are less effective in dark current suppression compared to **MD5** and **MD7** (vide infra, see EIS), leading to smaller photovoltages.

View Article Online
DOI: 10.1039/C8TA04774J

Consequently, **MD5** and **MD7** exhibit better conversion efficiencies than **MD4** and **MD6**. The largest dye loading amount and most efficient dark current suppression (vide infra) certainly contribute significantly to the best performance of **MD7** among all. In comparison, the lowest dye loading, most serious dye aggregation and largest dark current (vide infra) render the cell performance of **MD4** the lowest among all. Better performance of **MD6** than **MD4** (or **MD7** than **MD5**) can be attributed mainly to two reasons: (1) better light harvesting because of higher dye loading as well as broader and more intense absorption spectra (vide supra); (2) better dark current suppression, leading to marginal increment of the photovoltage.

The higher V_{OC} values of **MD4** and **MD6** than other **TP** dyes[14c,14d,27] using I^-/I_3^- redox mediator suggest more effective dark current suppression in the former owing to the bulky dihexyloxyphenyl moieties at the **TP** entity. Dihexyloxyphenyl moiety at the **BP** entity also benefits dark current suppression in **BP** dyes, as **MD5** and **MD7** have relatively higher photovoltages than their congeners without substituents at 2- and 3-site of **BP**, **FNE45** and **FNE46**.[32a] Among **BP** dyes with triphenylamine donor, the V_{OC} values of **MD5** and **MD7** also appear to be higher for DSSCs using I^-/I_3^- redox couple.[14a,25,32] Though the cell efficiencies of **MD5** (7.88%) and **MD7** (8.22%) are somewhat lower than the best efficiency (9.83%) reported for single **BP** dye,[33] they compete favorably with other triphenylamine-based **BP** dyes.[14a,25,32]

Adding co-adsorbent during dye soaking has been proven to help with anti-aggregation of the dyes in addition to passivation of TiO_2 surface for dark current suppression.[34] As there exists slight dye aggregation, addition of co-adsorbent was also tested. After adding 1 mM CDCA co-adsorbent, both V_{OC} and J_{SC} were improved and the power conversion efficiencies increased accordingly: **MD4**, 4.58%; **MD5**, 8.39%; **MD6**, 5.26%; **MD7**, 9.03%. The $J-V$ curves and IPCE plots with CDCA are shown in **Fig. 5c** and **Fig. 5d**, respectively. Both V_{OC} and J_{SC} increase in spite of decreasing dye loading, providing good evidence for alleviation of dye aggregation upon addition of CDCA. Accordingly, all dyes exhibit higher IPCE values after addition of CDCA.

Electrochemical impedance spectroscopy (EIS) taken in the dark was used to analyze the interfacial electron transfer properties in DSSCs. **Fig. 6a** shows the Nyquist plots for DSSCs based on **MD4**–**MD7** dyes. The semicircle with larger impedance is related to charge recombination resistance (R_{rec}) of the injected electron with the oxidized electrolyte occurring at the TiO_2/dye/electrolyte interface, and the larger R_{rec} means lesser tendency for recombination, i.e.

View Article Online
DOI: 10.1039/C8TA04774J

lower dark current. The R_{rec} value for sensitizers decreases in the order of **N719** (206 Ω) > **MD7** (171 Ω) > **MD5** (165 Ω) > **MD6** (139 Ω) > **MD4** (114 Ω), which is in agreement with the order of the dark current (**Fig. 6a**). The trend is also in line with that of V_{OC} value, **N719** (751 mV) > **MD7** (725 mV) > **MD5** (718 mV) > **MD6** (705 mV) > **MD4** (700 mV). The electron recombination lifetime extracted from the Bode phase plots (**Fig. 7b**) using $\tau_{rec} = 1/2\pi f$, **MD7** (40.83 ms) > **MD5** (18.73 ms) > **MD6** (12.94 ms) > **MD4** (7.96 ms), provides additional supporting evidence. The larger R_{rec} value of **BP** than **TP** dyes, i.e., **MD7** > **MD6** and **MD5** > **MD4**, may be attributed to two reasons: (1) more compact packing (higher dye loading) of the dyes on TiO_2, resulting in less free volume for penetration of the electrolytes to the TiO_2 surface; (2) the larger twist angles between **BP** and two neighboring thiophene rings than those between **TP** and the neighbouring thiophene rings, resulting in more effective blockade of the electrolytes from approaching the TiO_2 surface. The two alkoxy chains at the arylamine donor also help with dark current suppression, i.e., **MD7** > **MD5** and **MD6** > **MD4**. **MD7** stands out to be the best for dark current suppression due to its higher dye loading, twist structure and the presence of the alkoxy chains at the donor.

Table 2 Photovoltaic parameters of **MD** dyes with and without CDCA under AM 1.5G[a]

dye	η	V_{OC}	J_{SC}	*FF*	R_{rec}	τ_{rec}	dye loading
	%	V	mA cm^{-2}		Ω	ms	10^{-7}mol cm^{-2}
MD4	3.92 ± 0.02	0.631 ± 0.003	9.56 ± 0.02 (8.13)	0.65 ± 0.03	112	7.92	1.29
MD4[*]	4.58 ± 0.02	0.687 ± 0.004	10.11 ± 0.01 (8.65)	0.66 ± 0.01			1.01
MD5	7.88 ± 0.03	0.715 ± 0.002	16.50 ± 0.01 (15.05)	0.67 ± 0.03	163	19.41	3.10
MD5[*]	8.39 ± 0.02	0.727 ± 0.003	17.16 ± 0.03 (15.67)	0.67 ± 0.04			2.12
MD6	5.08 ± 0.03	0.695 ± 0.002	11.25 ± 0.01 (9.85)	0.65 ± 0.01	136	12.75	2.81
MD6[*]	5.26 ± 0.02	0.700 ± 0.004	11.58 ± 0.01 (10.16)	0.65 ± 0.02			2.02
MD7	8.22 ± 0.04	0.719 ± 0.002	17.12 ± 0.04 (15.78)	0.67 ± 0.02	172	37.91	5.03
MD7[*]	9.03 ± 0.02	0.753 ± 0.003	17.65 ± 0.01 (16.28)	0.68 ± 0.02			4.51
N719	8.87 ± 0.01	0.745 ± 0.001	17.50 ± 0.03	0.68 ± 0.01	204		

View Article Online
DOI: 10.1039/C8TA04774J

[a]V_{OC}: open-circuit voltage; J_{SC}: short-circuit current and the values in the parentheses are the products of the IPCE value at each wavelength and the photon flux density data listed in the AM 1.5 solar spectrum; *FF*: fill factor; *PCE*: power-conversion efficiency. The data are based on five measurements. Experiments were conducted by using TiO_2 photo-electrodes with approximately 12 μm thickness and 0.16 cm^2 working area on fluorine-doped tin oxide substrates. **MDn**: without CDCA; **MDn***: with CDCA where **n** = **4**, **5**, **6** and **7**.

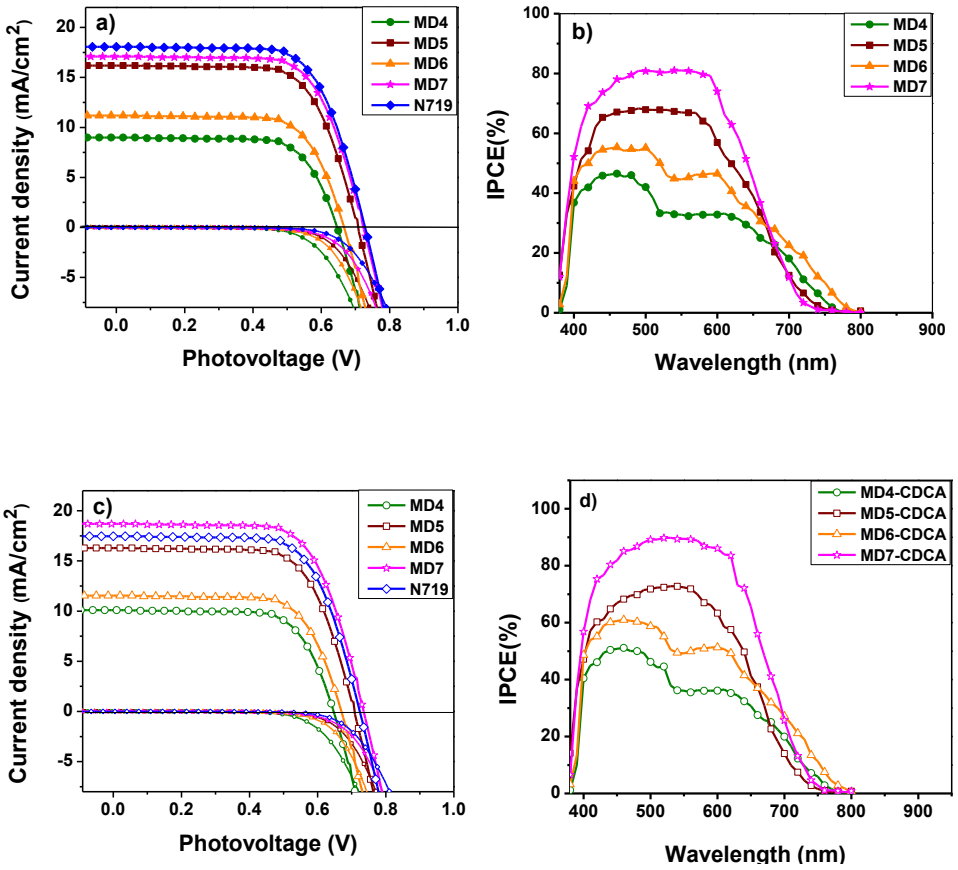

Fig. 5 (a) Current density-voltage (*J*–*V*) curves and (b) IPCE spectra without CDCA, and (c) *J*–*V* curves and (d) IPCE spectra with CDCA for the DSSCs measured under simulated AM 1.5G illumination.

View Article Online
DOI: 10.1039/C8TA04774J

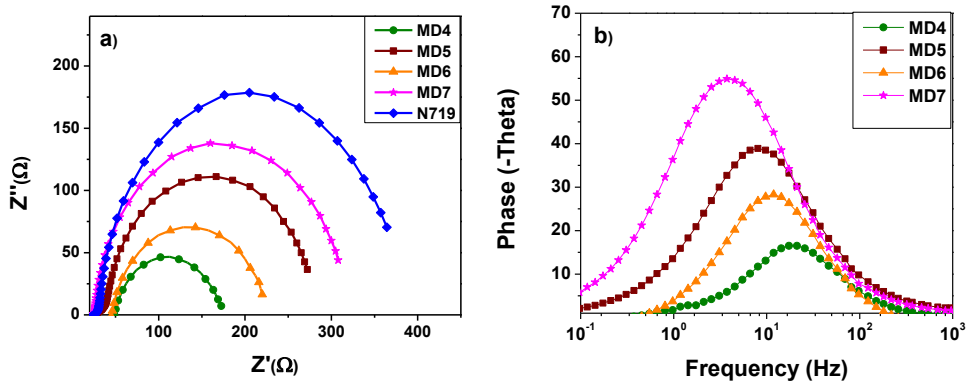

Fig. 6 Electrochemical impedance spectra, (a) Nyquist plots and (b) Bode plots of DSSCs based on the dyes **MD4**–**MD7** measured in the dark at applied bias of -0.7 V.

3.5 DSSCs Performance under Dim-Light Condition

Due to panchromatic absorption, the absorption spectra of **MD** dyes have good spectral coverage with the emission spectrum of the T5 fluorescence lamp (see **Fig. S7** in SI). The high photovoltage of the **MD** dyes should also be beneficial for dim light environments. The photovoltaic performance of **MD** dyes was therefore evaluated using T5 fluorescent lamp (0.1960 mW cm^{-2}) illumination with irradiance in the range of 300−6000 lux. CDCA (1 mM) was added as the co-adsorbent during dye soaking and I^-/I_3^- was used as the redox mediator for all the cells. The current density−voltage (*J*−*V*) curve of DSSCs under 300 lux T5 fluorescent light illuminationis shown in **Fig. 7** and **Table 3** displays the summarized dim-light cell efficiency data of the dyes at 300, 600, 900 and 6000 lux. The performance data for all other irradiance are compiled in **Table S8**. Both **BP**-based dyes (**MD5** and **MD7**) have cell efficiency of >15% even at only 300 lux illumination, and **MD7** has the best performance among all: 18.95% (300 lux), 20.16% (600 lux), 21.10% (900 lux) and 27.17% (6000 lux). The efficiencies are comparable with those of N719-based cell fabricated and measured under similar condition: 19.02% (300 lux), 20.23% (600 lux), 20.94% (900 lux) and 27.64% (6000 lux). The performance of **MD7**, though lower than the record efficiency reported by Freitag et. al. on a co-dyed system using Cu(II/I)(tmby) (tmby = 4,4',6,6'-tetramethyl-2,2'-bipyridine) as the redox mediator (25.5% at 200 lux; 28.9% at 1000 lux),[6a] is very competitive with the best cell based on single sensitizer and I^-/I_3^- redox couple reported by Tingare et. al.: 21.40% (300 lux), 21.88% (600 lux), 23.64% (900 lux) and 28.56% (6000 lux).[6c] Similar to the case of 1 sun illumination, the efficiencies of **TP**-based dyes (**MD4** and **MD6**) are

View Article Online
DOI: 10.1039/C8TA04774J

significantly lower: for **MD4**, 6.39% to 8.62% as the irradiance varies from 300 to 6000 lux; for **MD6**, 12.08% to 16.86% as the irradiance varies from 300 to 6000 lux. Based on the results at 1 sun, the lower V_{OC} values of **MD4** and **MD6** can be attributed to less effective dark current suppression, and lower J_{SC} values due to their less efficient electron injection.

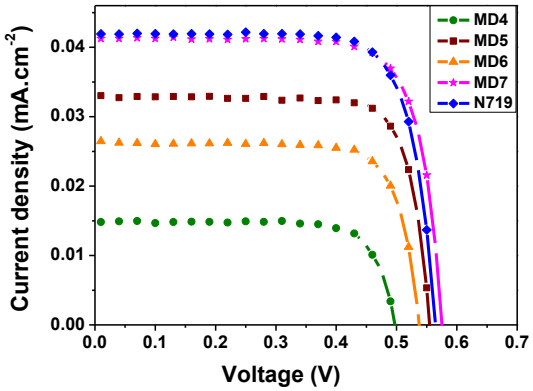

Fig. 7 Current density-voltage (*J*−*V*) curves for **MD** dyes under T5 illuminance (300 lux).

Table 3 Photovoltaic parameters of **MD** dyes measured using T5 fluorescent light[a]

dye	illuminance	irradiance	*Voc*	*Jsc*	*FF*	*η*
	Lux	mW cm^{-2}	mV	μA cm^{-2}	%	%
MD4	300	0.09	499.16 ± 2.61	15.49 ± 0.51	75.18 ± 0.91	6.39 ± 0.13
	600	0.18	516.03 ± 2.57	29.95 ± 0.13	75.58 ± 0.31	6.67 ± 0.11
	900	0.27	530.11 ± 0.69	44.82 ± 0.79	76.35 ± 0.13	6.81 ± 0.19
	6000	1.7	582.26 ± 5.09	315.06 ± 0.00	76.63 ± 0.06	8.62 ± 0.16
MD5	300	0.09	543.26 ± 18.25	33.47 ± 0.66	77.24 ± 2.01	15.10 ± 0.67
	600	0.18	568.20 ± 15.53	67.95 ± 1.07	77.73 ± 1.73	16.49 ± 0.40

View Article Online
DOI: 10.1039/C8TA04774J

	900	0.27	586.23 ± 16.40	104.61 ± 1.96	78.04 ± 1.67	17.38 ± 0.38
	6000	1.7	651.16 ± 10.24	762.13 ± 26.12	79.01 ± 1.27	23.17 ± 0.22
MD6	300	0.09	542.85 ± 7.68	26.87 ± 0.81	76.21 ± 0.94	12.08 ± 0.02
	600	0.18	561.95 ± 8.00	53.46 ± 1.19	77.05 ± 0.68	12.79 ± 0.05
	900	0.27	575.60 ± 9.52	80.72 ± 1.14	77.76 ± 1.01	13.24 ± 0.11
	6000	1.7	634.48 ± 8.30	562.20 ± 1.51	77.40 ± 0.82	16.86 ± 0.23
MD7	300	0.09	572.67 ± 3.79	40.92 ± 1.76	75.85 ± 0.68	18.95 ± 0.69
	600	0.18	596.77 ± 4.40	81.80 ± 2.15	76.59 ± 0.77	20.16 ± 1.10
	900	0.27	611.89 ± 4.22	124.33 ± 3.47	76.83 ± 0.83	21.10 ± 1.20
	6000	1.7	676.32 ± 6.32	913.69 ± 37.34	76.42 ± 0.38	27.17 ± 1.44
N719	300	0.09	550.53 ± 12.34	41.48 ± 0.51	75.34 ± 1.17	19.02 ± 0.70
	600	0.18	582.94 ± 13.91	82.17 ± 2.50	75.72 ± 1.50	20.23 ± 0.89
	900	0.27	597.55 ± 14.28	126.06 ± 4.43	75.72 ± 2.27	20.94 ± 1.06
	6000	1.7	676.37 ± 24.38	923.38 ± 27.29	75.85 ± 1.98	27.64 ± 0.54

[a] V_{OC}: open-circuit voltage; J_{SC}: short-circuit current; *FF*: fill factor; *PCE*: power-conversion efficiency. The data are based on three measurements. Experiments were conducted by using TiO_2

View Article Online
DOI: 10.1039/C8TA04774J

photoelectrodes, soaked with dyes and CDCA (1 mM), with approximately 12 μm thickness and 0.16 cm^2 working area on fluorine-doped tin oxide substrates.

4 Conclusions

We have developed four new D−A′−π−A type sensitizers (**MD4**−**MD7**) with thieno[3,4-*b*]pyrazines (**TP**) and benzo[3,4-*b*]pyrazine (**BP**) as the auxiliary acceptor. Incorporation of 3,4-dihexyloxyphenyl moiety at the 2- and 3-site of **TP** and **BP** improves the solubility of the dyes in organic solvents and helps with suppression of dark current in DSSCs. The best efficiency of 8.21% for **MD7** reaches 92% of **N719**-based standard cell. Addition of 1 mM CDCA as co-adsorbent helps with alleviation of dye aggregation and improvement of cell performance. Consequently, **MD7** has an efficiency of 9.00 %, which surpassed that of the **N719**-based cell. DSSCs based on **MD5** and **MD7** have cell efficiencies of >15% at 300 lux irradiance (T5 fluorescent light source). The cell efficiency of **MD7** reaches 18.95% at 300 lux and 27.17% at 6000 irradiance.

Associated Content

Supporting Information

It includes the synthesis procedures, ^{1}H NMR spectra, ^{13}C NMR spectra, Mass spectra , details of theoretical calculations and all necessary figures and tables of the new compounds.

Author information

*Corresponding Authors
E-mail: jtlin@gate.sinica.edu.tw, tcwei@mx.nthu.edu.tw.

Conflict of interest

There are no conflicts to declare

Acknowledgment

We thank the Academia Sinica (AS), National Tsing Hua University and Ministry of Science and Technology for financial support, and the Instrumental Center of Institute of Chemistry, AS.

References

View Article Online
DOI: 10.1039/C8TA04774J

[1] (a) Z. Yao, M. Zhang, H. Wu, L. Yang, R. Li and P. Wang, *J. Am. Chem. Soc.*, 2015, **137**, 3799–3802; (b) Z. Yao, H. Wu, Y. Li, J. Wang, J. Zhang, M. Zhang, Y. Guo and P. Wang, *Energy Environ. Sci.*, 2015, **11,** 3192–3197; (c) S. Mathew, A. Yella, P. Gao, R. Humphry-Baker, B. F. E. Curchod, N. Ashari-Astani, I. Tavernelli, U. Rothlisberger, M. K. Nazeeruddin and M. Grätzel, *Nat. Chem.*, 2014, **6**, 242–247; (d) Y. Ren, D. Sun, Y. Cao, H. N. Tsao, Y. Yuan, S. M. Zakeeruddin, P. Wang and M. Grätzel, *J. Am. Chem. Soc.*, 2018, **140**, 2405–2408; (e) K. Kakiage, Y. Aoyama, T. Yano, K. Oya, J. Fujisawa and M. Hanaya, *Chem. Commun.*, 2015, **51**, 15894–15897; (f) K. Kakiage, Y. Aoyama, T. Yano, T. Otsuka, T. Kyomen, M. Unnoc and M. Hanaya, *Chem. Commun.*, 2014, **50**, 6379–6381; (g) A. Yella, H.-W. Lee, H. N. Tsao, C. Yi, A. K. Chandiran, M. K. Nazeeruddin, E. W. -G. Diau, C. -Y. Yeh, S. M. Zakeeruddin and M. Grätzel, *Science*, 2011, **334**, 629–634; (h) A. Yella, C. -L. Mai, S. M. Zakeeruddin, S. -N. Chang, C. -H. Hsieh, C.-Y. Yeh and M. Grätzel, *Angew. Chem. Int. Ed.*, 2014, **53**, 2973–2977; (i) J. Wang, H. Wu, L. Jin, J. Zhang, Y. Yuan and P. Wang, *ChemSusChem*, 2019, **10**, 2962–2967; (j) Y. K. Eom, S. H. Kang, I. T. Choi, Y. Yoo, J. Kim and H. K. Kim, *J. Mater. Chem. A*, **2017**, *5*, 2297−2308; (k) S. H. Kang, M. J. Jeong, Y. K. Eom, I. T. Choi, S. M. Kwon, Y. Yoo, J. Kim, J. Kwon, J. H. Park and H. K. Kim, *Adv. Energy Mater.*, 2017, **7**, 1602117.

[2] B. O'Regan and M. Grätzel, *Nature*, 1991, **353**, 737–740.

[3] (a) A. Fakharuddin, R. Jose, T. M. Brown, F. Fabregat-Santiago and J. Bisquert, *Energy Environ. Sci.*, 2014, **7**, 3952–3981; (b) S. Yun, Y. Qin, A. R. Uhl, N. Vlachopoulos, M. Yin, D. Dongdong Li, X. Han and A. Hagfeldt, *Energy Environ. Sci.*, 2018, **11**, 476–526.

[4] P. Brogdon, H. Cheema and J. H. Delcamp, *ChemSusChem*, 2018, **11**, 86−103.

[5] (a) F. De Rossi, T. Pontecorvo and T. M. Brown, *Appl. Energy*, 2015, **156**, 413−422; (b) A. Sacco, L. Rolle, L. Scaltrito, E. Tresso and C. F. Pirri, *Appl. Energy*, 2013, **102**, 1295−1302; (c)

View Article Online
DOI: 10.1039/C8TA04774J

G. Kapil, Y. Ogomi, S. S. Pandey, T. Ma and S. Hayase, *J. Nanosci. Nanotechnol.*, 2016, **16**, 3183−3193.

[6] (a) M. Freitag, J. Teuscher, Y. Saygili, X. Zhang, F. Giordano, P. Liska, J. Hua, S. M. Zakeeruddin, J.-E. Moser, M. Grätzel and A. Hagfeldt, *Nat. Photonics*, 2017, **11**, 372−378; (b) C. -L. Wang, P. -T. Lin, Y. -F. Wang, C. -W. Chang, B. -Z. Lin, H. H. Kuo, C. -W. Hsu, S. -H. Tu and C.-Y. Lin, *J. Phys. Chem. C*, 2015, **119**, 24282−24289; (c) Y. S. Tingare, N. S. Vinh, H. -H. Chou, Y. -C. Liu, Y. -S. Long, T. -C. Wu, T. -C. Wei and C. –Y. Yeh,, *Adv. Energy Mater.*, 2017, **6**, 170032; (d) H. -H. Chou, Y. -C. Liu, G. Fang, Q. -K. Cao, T. -C. Wei and C. -Y. Yeh, *ACS Appl. Mater. Interfaces*, 2017, **9**, 37786−37796; (e) M. -C. Tsai, C. -L. Wang, C.-W. Chang, C.-W. Hsu, Y. -H. Hsiao, C. -L. Liu, C. -C. Wang, S. -Y. Lin and C. -Y. Lin, *J. Mater. Chem. A*, 2018, **6**, 1995−2003; (f) Y. -J. Lin, J. -W. Chen, P. -T. Hsiao, Y. -L. Tung, C. -C. Chang and C. -M. Chen, *J. Mater. Chem. A*, 2017, **5**, 9081−9089; (g) Y. -C. Liu, H. -H. Chou, F. -Y. Ho, H. -J. Wei, T. -C. Wei and C. -Y. Yeh, *J. Mater. Chem. A*, 2016, **4**, 11878−11887.

[7] (a) Y. Wu and W. Zhu, *Chem. Soc. Rev.*, 2013, **42**, 2039–2058; (b) Y. Wu, W. H. Zhu, S. M. Zakeeruddin and M. Grätzel, *ACS Appl. Mater. Interfaces*., 2015, **7**, 9307−9318.

[8] S. Chaurasia and J. T. Lin, *Chem. Record*, 2016, **16**, 1311−1336.

[9] M. Velusamy, K. R. J. Thomas, J. T. Lin, Y. -C. Hsu and K. -C. Ho, *Org. Lett.*, 2005, **7**, 1899–1902.

[10] S. Chaurasia, C. -Y. Hsu, H. -H. Chou and J. T. Lin, *Org. Electron.*, 2014, **15**, 378−390.

[11]S. Chaurasia, W. -I Hung, H. -H. Chou and J. T. Lin, *Org. Lett.*, 2014, **16**, 3052−3055.

[12] S. Chaurasia, C. -T. Li, M. B. Desta, J. -S. Ni, and J. T. Lin, *Chem. Asian J.*, 2017, ***12***, 996–1004.

View Article Online
DOI: 10.1039/C8TA04774J

[13] (a) C. Liu, K. Kang, X. Gong and A. J. Heeger, *Chem. Soc. Rev.*, 2016, **45**, 4825–4846; (b) J. Yuan, J. Ouyang, V. Cimrová, M. Leclerc, A. Najari and Y. Zou, *J. Mater. Chem. C*, 2017, **5**, 1858–1879; (c) D. Gedefaw, M. Prosa, M. Bolognesi, M. Seri and M. R. Andersson, *Adv. Energy Mater.*, 2017, **7**, 1700575.

[14] (a) L. -W. Ma, Z. -S. Huang, S. Wang, H. Meier and D. Cao, *Dyes Pigm.*, 2017, **145**, 126−135; (b) H. Zhu, B. Liu, J. Liu, W. Zhang and W. -H. Zhu, *J. Mater. Chem. C*, 2015, **3**, 6882-6890; (c) N. P. Liyanage, A. Yella, M. Nazeeruddin, M. Grätzel and J. H. Delcamp, *ACS Appl. Mater. Interfaces*, 2016, **8**, 5376−5384; (d) N. P. Liyanage, H. Cheema, A. R. Baumann, A. R. Zylstra and J. H. Delcamp, C*hemSusChem*, 2017, **10**, 2635–2641.

[15] (a) H. Tian, I. Bora, X. Jiang, E. Gabrielsson, K. M. Karlsson, A. Hagfeldt and L. Sun, *J. Mater. Chem.*, 2011, **21**, 12462−12472; (b) M. Katono, M. Wielopolski, M. Marszalek, T. Bessho, J. -E. Moser, R. Humphry-Baker, S. K. Zakeeruddin, M. Grätzel, *J. Phys. Chem.*, 2014, **111**, 16486−16493; (c) Y. K. Eom, S. H. Kang, I. T. Choi, Y. Yoo, J. Kim, and H. K. Kim, *J. Mater. Chem. A*, 2017, 5, 2297−2308; (d) Y. K. Eom, I. T. Choi, S. H. Kang, J. Lee, J. Kim, M. J. Ju, and H. K. Kim, *Adv. Energy Mater.*, 2015, **5**, 1500300.

[16] C. -T. Li, C. -P. Lee, M. -S. Fan, P. -Y. Chen, R. Vittal and K. -C. Ho, *Nano Energy*, 2014, **9**, 1–14.

[17] M. J. Frisch, G. W. Trucks, H. B. Schlegel, G. E. Scuseria, M. A. Robb, J. R. Cheeseman, G. Scalmani, V. Barone, B. Mennucci, and G. A. Petersson, Gaussian 09, Revision B.01, Gaussian, Inc., Wallingford, CT, 2010. http://gaussian.com/glossary/g09/.

[18] G. A. Petersson, A. Bennett, T. G. Tensfeldt, M. A. Al-Laham, W. A. Shirley and J. Mantzaris, *J. Chem. Phys.*, 1988, **89**, 2193–2198.

[19] M. Cossi, V. Barone, R. Cammi and J. Tomasi, *Chem. Phys. Lett.*, 1996, **255**, 327–335.

View Article Online
DOI: 10.1039/C8TA04774J

[20]N. M. O'Boyle, A. L. Tenderholt and K. M. Langner, *J. Comput. Chem.*, 2008, **29**, 839–845.

[21] J. Kim, S. H. Park, J. Kim, S. Cho, Y. Jin, J. Y. Shim, H. Shin, S. Kwon, I. Kim, K. Lee, A. J. Heeger and H. Suh, *J. Polym. Sci Polym. Chem.*, 2011, **49**, 369–380.

[22] T. -T. Bui, O. Thiebaut, E. Grelet, M. -F. Achard, B. G. Garreau-de Bonneval and K. I. Moineau-Chane Ching. *Eur. J. Inorg. Chem.*, 2011, 2663–2676.

[23] M. Velusamy, K. R. J. Thomas, J. T. Lin, Y.-C. Hsu and K.-C. Ho, *Org. Lett.*, 2005, **7**, 1899-1902.

[24] X. Lu, S. Fan, J. Wu, X. Jia, Z.-S. Wang and Zhou, G. *J. Org. Chem.*, 2014, **79,** 6480-6489.

[25] S. -R. Li, C. -P. Lee, C. -W. Liao, W. -L. Su, C. -T. Li, K. -C. Ho, and S. -S. Sun, *Tetrahedron*, 2014, **70**, 6276-6284.

[26] S. -R. Li, C. -P. Lee, P. -F. Yang, C. -W. Liao, M. -M. Lee, W. -L. Su, C. -T. Li, H. -W. Lin, K. -C. Ho and S. -S. Sun, *Chem. Eur. J.*, 2014, **20,** 10052-10064.

[27] J. Wu, G. Li, L. Zhang, G. Zhou and Z. -S. Wang, *J. Mater. Chem. A*, 2016, **4,** 3342-3355.

[28] X. Lu, X. Jia, Z. S. Wang and G. Zhou, *J. Mater. Chem. A*, 2013, **1,** 9697-9706.

[29] H. Choi, J. K. Lee, K. Song, S. O. Kang and J. Ko, *Tetrahedron*, 2007, **63,** 3115-3121.

[30] M. Grätzel, *Nat*ure, 2001, **414,** 338-344.

[31] A. Hagfeldt and M.Grätzel, *Chem. Rev*., 1995, **95**, 49-68.

[32] (a) X. Lu, Q. Feng, T. Lan, G. Zhou and Z.-S. Wang, *Chem. Mater.*, 2012, **24,** 3179-3187; (b)S. -R. Li, C. -P. Lee, P. -F. Yang, C. -W. Liao, M. Lee, W. -L. Su, C. -T. Li, H.-W. Lin, K. -C. Ho and S. -S. Sun, *Chem. Eur. J.*, 2014, **20,** 10052-10064; (c) J. -X. Cheng, Z. -S. Huang, L. Wang and D. Cao, *Dyes Pigm.*, 2016, **131,** 134-144.

[33] Y. Wang, Z. Zheng, T. Li, N. Robertson, H. Xiang, W. Wu, J. Hua, W.H. Zhu and H. Tian, *ACS Appl. Mater. Inter.*, 2016, **8**, 31016-31024.

View Article Online
DOI: 10.1039/C8TA04774J

[34] (a) S. Zhang, X. Yang, C. Qin, Y. Numata and L. Han, *J. Mater. Chem. A.*, 2014, *2*, 5167-5177; (b) J. Li, W. Wu, J. Yang, J. Tang, Y. Long and J. Hua, *Sci. China Chem.*, 2011, **54,** 699-706.

View Article Online
DOI: 10.1039/C8TA04774J

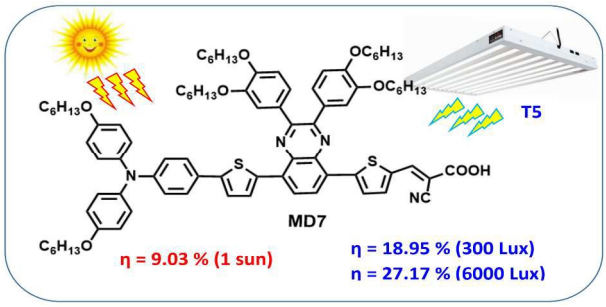

DSSCs fabricated from benzo[3,4-*b*]pyrazine-based metal-free sensitizer have efficiencies of 9.03% at 1 sun and 18.95% at 300 lux irradiance.